A HTAP multi-model assessment of the influence of regional anthropogenic emission reductions on aerosol direct radiative forcing and the role of intercontinental transport

Hongbin Yu[1,2], Mian Chin[2] , J. Jason West[3] , Cynthia S. Atherton[4] , Nicolas Bellouin[5] , Dan Bergmann[4] , Isabelle Bey[6] , Huisheng Bian[7,2] , Thomas Diehl[8,2] , Gerd Forberth[5] , Peter Hess[9] , Michael Schulz[10] , Drew Shindell[11] , Toshihiko Takemura[12] , Qian Tan[8,2]

1. Earth System Science Interdisciplinary Center, University of Maryland, College Park, Maryland, 20740, USA
2. Earth Science Directorate, NASA Goddard Space Flight Center, Greenbelt, Maryland, 20771, USA
3. Department of Environmental Sciences and Engineering, University of North Carolina, Chapel Hill, NC 27599, USA
4. Atmospheric Earth and Energy Division, Lawrence Livermore National Laboratory, Livermore CA 94551, USA
5. Met Office Hadley Centre, FitzRoy Road, Exeter Devon, EX1 3PB, UK
6. Center for Climate Systems Modeling, ETH Zurich, Universitätstrasse 16, 8092 Zürich, Switzerland
7. Joint Center for Earth Systems Technology, University of Maryland at Baltimore County, Baltimore, Maryland, 21228, USA
8. Universities Space Research Association, Columbia, Maryland, 21044, USA
9. Biological and Environmental Engineering, Cornell University, Ithaca, New York, 14850, USA
10. Meteorologisk Institutt, Postboks 43 Blindern 0313, Oslo, Norway
11. NASA Goddard Institute for Space Studies, New York, New York, 10025, USA
12. Research Institute for Applied Mechanics, Kyushu University, Japan

Correspondence

Hongbin Yu
NASA GSFC Code 613
Greenbelt, MD 20771, USA
Hongbin.Yu@nasa.gov
301-614-6209

Abstract In this study, we assess changes of aerosol optical depth (AOD) and direct radiative forcing (DRF) in response to the reduction of anthropogenic emissions in four major pollution regions in the northern hemisphere by using results from 10 global chemical transport models in the framework of the Hemispheric Transport of Air Pollution (HTAP). The multi-model results show that on average, a 20% reduction of anthropogenic emissions in North America, Europe, East Asia and South Asia lowers the global mean AOD and DRF by about 9%, 4%, and 10% for sulfate, organic matter, and black carbon aerosol, respectively. The impacts of the regional emission reductions on AOD and DRF extend well beyond the source regions because of intercontinental transport. On an annual basis, intercontinental transport accounts for 10-30% of the overall AOD and DRF in a receptor region, with domestic emissions accounting for the remainder, depending on regions and species. While South Asia is most influenced by import of sulfate aerosol from Europe, North America is most influenced by import of black carbon from East Asia. Results show a large spread among models, highlighting the need to improve aerosol processes in models and evaluate and constrain models with observations.

1. Introduction

Anthropogenic aerosols make significant contributions to the global mean radiative forcing (RF) of climate *[Forster et al., 2007]* by scattering and absorbing solar radiation (so-called "aerosol direct effects") *[McCormick and Ludwig, 1967]* and modifying cloud properties, amount, and evolution (collectively referred to as "aerosol indirect effects") *[Twomey, 1977; Gunn and Phillips, 1957; Albrecht, 1989]*. RF is a measure of the change of net radiation (incoming minus outgoing) at the top of atmosphere (TOA), at the surface, or within the atmosphere, due to perturbations in atmospheric compositions or surface properties. On a global average basis, the sum of direct and indirect RF at TOA by anthropogenic aerosol is estimated to be -1.2 W m^{-2} [-2.4 to -0.6 W m^{-2}] (cooling) over the period of 1750-2000, which is significant compared to the positive (warming) forcing of +2.63 [±0.26] W m^{-2} by anthropogenic long-lived greenhouse gases over the same period *[Forster et al., 2007]*. In heavily polluted regions, aerosol cooling overwhelms greenhouse warming *[Ramanathan et al., 2001; Li et al., 2010]*. At the surface, aerosol RF can be much stronger than that at TOA because of aerosol absorption *[Satheesh and Ramanathan, 2000]*. Currently, uncertainties associated with aerosol RF make the largest contribution to the overall uncertainty in anthropogenic radiative forcing of climate *[Forster et al., 2007]*. Because of the significant role of aerosols in modulating the Earth's radiative budget, it is necessary from both scientific and policy perspective to assess how emission changes associated with economic development and regional/national regulations will influence the aerosol radiative forcing.

77 The response of global aerosol RF to a fractional change of anthropogenic emissions
78 would depend on the source locations, magnitude, and composition of emitted aerosols
79 and aerosol precursors. While scattering aerosols like sulfate cause a cooling effect,
80 strongly absorbing black carbon aerosols cause warming. Aerosol RF is also determined
81 by several environmental factors such as surface albedo and meteorological conditions
82 (in particular the amount and distribution of clouds and winds). With these differences,
83 the aerosol RF per unit change of regional emissions would differ from one region to
84 another. It is also important to note that the impact of a regional emission reduction is not
85 confined to the region itself. Instead regional emission reductions can have far reaching
86 impacts on RF in downwind regions, because of intercontinental transport of
87 anthropogenic aerosols. Long-range transport has been observed by long-term surface
88 monitoring networks *[Prospero et al., 2003; VanCuren, 2003; Fischer et al., 2010]*, in-
89 situ measurements from intensive field campaigns *[Ramanathan et al., 2007; Clarke and*
90 *Kapustin, 2010]*, and satellite observations *[Yu et al., 2008; Rudich et al., 2008; Dirksen*
91 *et al., 2009]* backed by model simulations [*Heald et al., 2006; Chin et al., 2007; Hadley*
92 *et al., 2007]*. Thus how a region is influenced by extraregional emissions is of particular
93 importance for formulating an effective strategy for mitigating regional climate change
94 and combating air pollution. The United Nations Economic Commission for Europe has
95 established a Task Force on Hemispheric Transport of Air Pollutants (HTAP) to
96 understand the growing body of scientific evidence of intercontinental transport and
97 assess its impacts on air quality, climate, and ecosystems *[HTAP, 2010]*.
98

Modeling studies can offer valuable insights into the relative significance of aerosols from different regions in influencing climate and important implications for formulating effective emission control strategies. Several recent studies have assessed how aerosols emitted in a region or from specific sectors could affect climate in downwind regions *[e.g., Reddy and Boucher, 2007; Koch et al., 2007; Shindell et al., 2008a, 2008b]*. Other studies have shown that large intermodel differences exist in aerosol lifetime cycle and radiative effect *[Kinne et al., 2006; Schulz et al., 2006; Textor et al., 2006],* which might undermine the robustness of the results from single model or very limited number of models. Complementary to the prior studies, we use in this study an ensemble of 10 global chemical transport or general circulation models to assess the change of global and regional aerosol optical depth (AOD) and direct radiative forcing (DRF) in response to 20% reductions of emissions from four major polluted regions in the Northern Hemisphere. These models conducted aerosol source-receptor (S/R) relationship experiments in the HTAP coordinated studies (HTAP 2010). These multi-model S/R experiments allow us to examine a probable range of contributions of intercontinental transport (ICT) relative to intra-regional emissions in determining regional AOD and DRF and help characterize the robustness of the results. Fry et al. *[2012]* conduct similar analysis of ozone radiative forcing due to 20% reductions of ozone precursor emissions using results from multiple HTAP models.

The rest of this paper is organized as follows. Section 2 describes the S/R model simulations and analysis methodology, including AOD from the HTAP anthropogenic S/R experiment used in this study and an estimate of the aerosol DRF. Section 3 presents

a multi-model analysis of the impacts of 20% reductions of regional anthropogenic emissions on global and regional AOD and DRF and the role of ICT relative to intra-regional emissions. This assessment does not address aerosol indirect effects, or warming effects resulting from BC deposition on snow and ice. We also neglect interactions of aerosols with thermal infrared radiation, as anthropogenic aerosols have relatively small size and their interactions with infrared radiation are minor. Finally, we neglect the radiative forcing of gas-phase components that may have been influenced by these emissions, which were modeled by Fry et al. (2012). Major conclusions from the analysis are summarized and discussed in Section 4.

2. Description of model simulations and analysis methodology

2.1. HTAP modeling experiments on S/R relationships

We use the results from an ensemble of 10 global chemical transport or general circulation models, listed in **Table 1**, to evaluate changes in AOD and DRF in response to a 20% reduction of anthropogenic emissions in four major pollution regions in the Northern Hemisphere under the framework of the HTAP S/R modeling experiments *[Fiore et al., 2009; HTAP, 2010]*. The S/R experiments include a baseline simulation and four perturbation simulations, for which each model submitted monthly AOD fields. For each model, the baseline simulation (SR1) is conducted using emissions and meteorology for 2001. Note that individual models use their own preferred anthropogenic and natural emissions. Each of the four perturbation runs (SR6) represents a 20% reduction in anthropogenic emissions (including biomass burning and n=both gas-phase and aerosol components) in one of four major pollution regions in Northern Hemisphere, namely

North America (NA), Europe (EU), East Asia (EA), and South Asia (SA), as illustrated in **Figure 1.** These perturbation model experiments are denoted as SR6NA, SR6EU, SR6EA, and SR6SA, respectively. Also shown in Figure 1 are regional and annual anthropogenic emissions of sulfur dioxide (SO_2), primary particulate organic matter (POM), and black carbon (BC) from 8 models (emissions for ECHAM5 and HadGEM2 were not archived and can not be retrieved for this analysis). Clearly anthropogenic emissions show large regional differences. For example, South Asia has the least SO_2 emissions that are a factor of 2-4 smaller than the other regions. East Asia has the largest BC emissions that are nearly double the emissions in Europe or South Asia and more than triple the emissions in North America. The regional differences in emissions in combination with the proximity of regions (e.g., the SA region is adjacent to and downwind of the EU region), ICT pathways, and removal/production mechanisms during the transport, would determine the relative roles of ICT and regional emissions, as we will discuss later in the paper.

2.2 AOD from HTAP S/R experiments

The major HTAP model outputs used in this study are monthly average AOD (τ) at 550 nm for sulfate (SO_4), POM, and BC from individual models. **Figure 2** shows annual average AOD in ambient conditions for a combination of SO_4, POM, and BC from 9 models. ECHAM5 simulations are not shown here because the model calculates AOD for dry sulfate, POM, and BC. Although the model also provides water optical depth associated with total aerosol (e.g., due to aerosol humidification), it is impossible, without further uncertain assumptions, to partition the water optical depth into that

168 associated with individual aerosol components. Note that these AOD outputs include both
169 anthropogenic and natural contributions (e.g., DMS derived sulfate AOD and biomass
170 burning AOD, among others). The AOD distributions clearly show several hotspots
171 representing well-known industrial pollution regions (e.g., East and South Asia, Western
172 Europe, and eastern US) and biomass burning regions (e.g., equatorial Africa in DJF,
173 South America and southern Africa in JJA and SON). In **Table 2,** the global annual mean
174 AOD is 0.0335 ± 0.0134 (average ± standard deviation of the 9 models), 0.0108 ±
175 0.0047, and 0.0022 ± 0.0024 for SO_4, POM, and BC, respectively. Clearly AOD shows
176 large model diversity with the standard deviation equivalent to about half of the multi-
177 model average. These global annual means are lower than those from multiple model
178 simulations with harmonized emissions under the framework of the Aerosol Comparisons
179 between Observations and Models (AeroCom) *[Schulz et al., 2006]* by 10%, 28%, and
180 8% for sulfate, POM, and BC, respectively.
181
182 **Figure 3(a)** shows the 9-model median AOD for sulfate, POM, and BC combined as
183 derived from the SR1 baseline simulations and its comparisons with anthropogenic AOD
184 derived from MODIS over-ocean measurements using two different methods described
185 by Yu et al. *[2009]* (**Figure 3b,** denoted as MODIS-YU09) and Bellouin et al. *[2008]*
186 (**Figure 3c,** denoted as MODIS-BE08). MODIS-YU09 anthropogenic AOD is derived
187 from MODIS over-ocean retrievals of AOD and fine-mode fraction (FMF) using the
188 representative FMF values for individual aerosol types, which are determined from
189 MODIS observations in selected regions where the specific aerosol type predominates
190 *[Yu et al., 2009]*. MODIS-BE08 is derived from the same MODIS measurements, but

191 with the use of prescribed, in situ measurement-based thresholds of FMF for different
192 aerosol types (which are different from those derived from MODIS observations as in Yu
193 et al., 2009) aided by the satellite observed absorbing aerosol index to separate
194 anthropogenic aerosol from mineral dust and sea salt *[Bellouin et al., 2008]*. Deriving
195 anthropogenic AOD from satellite measurements over land is not currently feasible. As
196 shown in Figure 3, anthropogenic AOD of MODIS-YU09 is generally larger than
197 MODIS-BE08 AOD in northern hemispheric mid-latitudes. In the tropics, MODIS-BE08
198 AOD is somewhat higher than MODIS-YU09. Except for trans-Pacific transport in
199 spring, the cross-ocean transport from major industrial pollution and biomass burning
200 regions is generally more extensive in the HTAP model simulations than both MODIS-
201 based estimates. In particular, the models simulated significant cross-Atlantic transport of
202 tropical African smoke to South America in boreal winter, which is not clearly seen in the
203 MODIS-based estimates. **Figure 4** further compares zonal variations of HTAP seasonal
204 AOD for the sulfate, POM and BC mixture against that of the MODIS anthropogenic
205 AOD over the ocean in mid-latitudes (20-60ºN) of the Northern Hemisphere, where the
206 major intercontinental transport paths occur. Significant regional and seasonal differences
207 exist between the HTAP models and MODIS observations and between MODIS-YU09
208 and MODIS-BE08. In the North Atlantic, the MODIS anthropogenic AOD from both
209 methods is often near the low bound of 9 HTAP models. In the North Pacific, MODIS-
210 YU09 anthropogenic AOD generally agrees well with the median of HTAP models. On
211 the other hand, MODIS-BE08 is consistently lower than MODIS-YU09 and generally
212 entails the low bound of the HTAP model simulations, particularly in the northeastern
213 Pacific. The differences between the two MODIS-based estimates of anthropogenic AOD

result from the differences in specifics of the approaches, as discussed in Yu et al. *[2009]*. The pronounced differences between the two MODIS-based estimates of anthropogenic AOD manifest the urgent need to develop independent approaches based on other satellite measurements, and more importantly, to conduct in situ measurements of anthropogenic AOD over large scales *[Yu et al., 2009]*.

2.3 Estimate of the aerosol direct radiative forcing

Because the aerosol direct radiative forcing or the aerosol optical properties (i.e., single-scattering albedo and asymmetry factor) for calculating the forcing are not archived under the HTAP S/R experiment protocol, we estimate here the aerosol DRF for each model and component (i.e., sulfate, POM, or BC) as follows:

$$DRF_i(x, y, t) = AOD_i(x, y, t) \bullet NDRF_i(x, y, t) \qquad (i = SO_4, POM, \text{and } BC) \quad (1)$$

where x, y, and t represents longitude, latitude, and month, respectively, and NDRF is the normalized DRF with respect to AOD at 550 nm *[Zhou et al., 2005]*. In this study we derive monthly average $NDRF_i$ over each model grid cell by dividing the DRF by the AOD, using 2001 monthly average AOD and direct radiative forcing calculated from the Goddard Chemistry Aerosol Radiation and Transport (GOCART) model *[Chin et al., 2002]*. We then apply this $NDRF_i$ to the monthly average component AOD_i from the other models in the HTAP S/R experiments. We also estimate DRF for an external mixture of SO_4, POM and BC by simply summing up the DRF for individual components. Note that RF for an internal mixture could differ significantly from that for an external mixture *[Jacobson, 2001; Chung and Seinfeld, 2002]*. Although DRF does not increase with AOD in a fully linear manner over the whole range of AOD, the use of

237 the above linear formula to derive DRF and its change in response to a 20% reduction of
238 emissions would not introduce large uncertainties with respect to regional differences in
239 DRF *[Zhou et al., 2005; Anderson et al., 2005]*.
240
241 The GOCART model currently prescribes particle size distributions and refractive indices
242 for individual components based on the Optical Properties of Aerosols and Clouds
243 (OPAC) database *[Hess et al., 1998]*. Aerosol properties such as AOD, single scattering
244 albedo, and asymmetry factor are then calculated using the Mie code *[Chin et al., 2002,*
245 *2009]*. These aerosol optical properties along with surface albedos and cloud fields from
246 the Goddard Earth Observing System (GEOS) Data Assimilation System - Version 4 are
247 then used to drive the NASA Goddard radiative transfer model *[Chou et al., 1998]*. The
248 time step for the radiative transfer calculations is 30 min, which can adequately capture
249 the dependence of DRF on solar zenith angle *[Yu et al., 2004]*. For a specific component
250 (e.g., SO_4, POM, or BC), DRF is calculated as the difference of net downward radiative
251 flux between a radiative transfer calculation including all aerosol components and one
252 with the specific component excluded. This DRF is therefore different from the DRF
253 estimated in Forster et al. *[2007]*, where the reference is pre-industrial aerosols. In this
254 study, the GOCART DRF is calculated for solar radiation only and averaged over a 24-
255 hour period. GOCART calculations of DRF have been evaluated against remote sensing
256 measurements and other model simulations *[e.g., Yu et al., 2004; Yu et al., 2006]*.
257
258 **Table 3** lists the annual mean NDRF in the four defined regions and globally. For purely
259 scattering SO_4, NDRF is nearly the same at the top of atmosphere (TOA) and at the

surface. Because POM is partially absorbing in the UV range *[Chin et al., 2009]*, the surface NDRF is more negative than the TOA NDRF. BC aerosol is strongly absorbing over the whole solar spectrum, thus its TOA forcing is positive (i.e., TOA warming), while the surface forcing is strongly negative (i.e., surface cooling). Clearly BC aerosol is much more effective in interacting with solar radiation than SO_4 and POM, although it is typically associated with lower AODs. For a specific component, the difference in NDRF among regions is generally within 20-30%, due to the combined effects of differences in solar zenith angle, surface albedo, and cloud fields *[Yu et al., 2006]*. The global annual mean all-sky TOA NDRF is -24.2, -30.0, and +85.9 $Wm^{-2}\tau^{-1}$ for SO_4, POM, and BC, respectively. These values fall within the ranges reported in the literature, i.e., -10 ~ -32 $Wm^{-2}\tau^{-1}$ for SO_4, -5 ~ -38 $Wm^{-2}\tau^{-1}$ for POM, and +22 ~ +216 $Wm^{-2}\tau^{-1}$ for BC *[CCSP, 2009]*.

To apply the GOCART-based monthly $NDRF_i$ to the HTAP models, we regrid the component AOD_i from each model to a unified spatial resolution of 2°x2.5° and use eq. (1) to estimate the corresponding DRF_i. For the SR1 experiment and on a global and annual basis, the 9 models give the mean all-sky TOA DRF of -0.67 ± 0.28, -0.26 ± 0.13, and +0.22 ± 0.13 Wm^{-2} for SO_4, POM, and BC, respectively. Correspondingly, the respective DRF at the surface and in all-sky (including both cloudy and cloud-free) condition is -0.64 ± 0.26, -0.37 ± 0.19, and -0.43 ± 0.22 Wm^{-2}. When the anthropogenic fraction of AOD, e.g., 55%, 53%, and 100% respectively for SO_4, POM, and BC on a global and annual average basis *[Schulz et al., 2006]* is considered, our DRF estimates shown above are in good agreement with anthropogenic TOA DRF of -0.35 ± 0.15 Wm^{-2}

283 (SO_4), -0.13 ± 0.05 Wm^{-2} (POM), and +0.25 ± 0.09 (BC) Wm^{-2} reported by *Schulz et al.*
284 *[2006]*. The aerosol direct radiative forcing exhibits large regional and seasonal
285 variations, as shown in **Figure 5** for the all-sky DRF and for the external mixture of SO_4,
286 POM, and BC, as derived from the 9-model SR1 simulations. Over major industrial
287 pollution regions in northern hemispheric mid-latitudes, aerosol DRF can be as large as -
288 6 Wm^{-2} at TOA and -25 Wm^{-2} at the surface. The forcing is greater in JJA and MAM
289 than in DJF and SON. Similar magnitudes of DRF are seen in the tropics where biomass
290 burning smoke is dominant. The seasonal variations of DRF reflect the peak seasons of
291 biomass burning, e.g., DJF in the Sahel and JJA and SON in southern Africa and South
292 America.
293
294 We note that the use of GOCART-based NDRF is likely to understate the model diversity
295 in DRF, in comparison to that derived from full radiative transfer calculations by
296 participating models. Although other aerosol models currently use the OPAC to
297 characterize aerosol microphysical and optical properties just like GOCART, models can
298 differ substantially in aerosol vertical distributions, meteorological fields (such as relative
299 humidity, cloud distributions, and surface albedos), and radiative transfer schemes. These
300 differences combined may lead to large model differences in DRF. This could
301 particularly be the case for all-sky TOA DRF by BC, which depends strongly on the
302 vertical distributions of aerosol and clouds, as evidenced by the reported wide range of
303 DRF *[CCSP, 2009]*.
304

3. Influences of regional anthropogenic emission reductions on AOD and DRF

In this section we present how the 20% reduction of regional anthropogenic emissions changes AOD and DRF by analyzing differences between a set of SR6 experiments (SR6NA, SR6EU, SR6EA, and SR6SA) and the SR1 experiment. We examine first the changes in global mean AOD and DRF and then the spatial extents of AOD and DRF changes resulting from regional anthropogenic emission reductions. The relative roles of ICT and regional emissions are assessed with a concept of the relative annual intercontinental response (RAIR) (as defined in HTAP, 2010). For the reasons discussed earlier in 2.2, we exclude ECHAM5 results in the analysis of AOD and DRF magnitude. Because RAIR is less sensitive to water optical depth than AOD is, we include ECHAM5 results in the RAIR analysis.

3.1. Global mean

Just as aerosol radiative forcing varies regionally, the effects of changes in emissions of aerosols and their precursors on global mean DRF also varies with region. **Tables 4** and **5** list respectively changes of global annual average AOD and all-sky DRF in response to the 20% reduction of anthropogenic emissions in the four HTAP anthropogenic source regions. The combined impact of the 20% reduction of emissions in all of the four regions is to decrease AOD and DRF by about 9%, 4%, and 10% for sulfate, POM, and BC, respectively. Relative contributions from individual regions vary considerably. For sulfate, the change of global average AOD and DRF due to the reduction of SO_2 emissions in South Asia is substantially smaller than that due to the emission reductions

328 from the other regions. This is mainly because SO_2 emissions in the SA region are much
329 smaller than those in other regions (see Figure 1). For POM, the reductions of global
330 mean AOD and DRF due to the regional emission reduction are generally consistent with
331 regional differences in primary POM emissions. For BC, the reduction of emissions in
332 East Asia makes the largest contribution to the change of global average DRF, mainly
333 because of the highest BC emissions among the four regions. For the external mixture of
334 SO_4, POM, and BC, the 20% reductions in the anthropogenic emissions in the four
335 regions collectively yield the respective reductions of 0.0035, 45.5 mWm^{-2}, (1 mWm^{-2} =
336 10^{-3} Wm^{-2}) and 104.1 mWm^{-2} for global mean AOD, all-sky DRF at TOA and at the
337 surface, which represents respectively about 8%, 6% and 7% reduction from the baseline
338 simulation. Note that uncertainties are larger than given by the standard deviation in
339 Table 5, due to the use of NDRF from a single model, as discussed earlier.
340
341 Will the same amount of emission reduction in different regions introduce the same
342 change in global mean aerosol radiative forcing? To address this question, we calculate
343 the forcing efficiency with respect to emissions by normalizing the global annual mean
344 DRF difference between the SR6 and SR1 runs by the change (20%) in regional
345 emissions for each model, as shown in **Table 6**. For SO_4 and POM, we use the emissions
346 for SO_2 and primary POM respectively to calculate the forcing efficiency. These derived
347 forcing efficiency numbers should be considered as rough estimates, because some
348 models with fully coupled chemistry include changes of SO_4 resulting from the
349 reductions of other anthropogenic emissions (Fry et al., 2012) and a fraction of POM is
350 secondary aerosol formed from volatile organic carbon emissions. Clearly the forcing

efficiency for BC is an order of magnitude higher than that for SO_4 and POM, suggesting that BC emission control is a candidate for producing a large, near-term cooling that counters the warming of greenhouse gases. Despite wide model differences in the absolute value of forcing efficiency, several regional dependences appear to be rather robust among the models. As shown in **Figure 6,** all eight models consistently yield a smaller sulfate forcing efficiency for EA emissions than for EU emissions, which is consistent with the oxidant limitation in EA that reduces the efficiency of SO_2-to-sulfate transformation *[Koch et al., 2007]*. The models also consistently give the largest BC forcing efficiency for EU emissions. These results may have important implications for regional emission controls and their influences on global climate, which will be discussed in section 4.

3.2. Spatial extents and the role of ICT

The spatial extents of the AOD and DRF due to the reduction of regional emissions and the role of aerosol ICT are revealed by differencing SR6 and SR1 experiments. **Figure 7** shows the 9-model annual average changes of AOD and all-sky DRF by the external mixture of SO_4, POM, and BC, resulting from the 20% reduction of anthropogenic emissions over the four regions. Clearly emissions from North America, Europe, and East Asia exert significant DRF on intercontinental and even hemispheric scales. Emissions from South Asia have relatively small impacts mainly over the Indian Ocean and the tropical Pacific. The influences of regional emission reduction on AOD and DRF also depend on season. As an example, **Figure 8** shows seasonal variations of changes of the all-sky surface DRF between SR1 and SR6. Similar seasonal variations occur for AOD,

374 all-sky DRF at TOA and clear-sky DRF, which will not be discussed separately. For
375 North America, Europe, and East Asia, the 20% reduction of emissions in each region
376 decreases the direct forcing (i.e., less negative) by a larger amount and over more
377 extensive areas in summer and spring than in winter and fall. For comparison, the
378 influence of the 20% reduction of emissions in South Asia shows relatively small
379 seasonal variations.
380
381 To quantify the role of aerosol ICT in affecting regional climate forcing, we adopt a
382 concept of the RAIR as defined in HTAP *[2010]*. For AOD, RAIR in a receptor region i
383 is expressed as follows:
384
385 $$RAIR_i = \frac{\sum_j \delta AOD_{ji}}{\delta AOD_{ii} + \sum_j \delta AOD_{ji}} \qquad (j \neq i)$$
386
387 where index j represents a source region. δAOD_{ii} represents a change of AOD in the
388 receptor/domestic region i due to the emission reduction in the region itself and δAOD_{ji}
389 represents a change of AOD in the receptor i induced by the emission reduction in a
390 source region j outside of the receptor (or foreign region). Similarly, RAIR can be
391 defined for DRF, near-surface concentration, and surface deposition. By definition, RAIR
392 in a receptor region represents the percentage contribution of the intercontinental
393 transport of foreign emissions relative to the sum of foreign and domestic emissions.
394
395 We calculate the RAIR for AOD and DRF for individual models and then obtain multi-
396 model averages, as shown respectively in **Figure 9** and **10** with the columns representing

10-model (including ECHAM5) average and error bars indicating ±1 standard deviation of the model simulations. Clearly values of RAIR depend on both region and component. For all regions and components, the import from intercontinental transport is significant but local emissions remain the main contributor, with RAIR ranging from 10 to 30%. South Asia is most influenced by the import of sulfate aerosol, and North America is most influenced by the import of BC, followed by POM. For sulfate, POM, and BC combined, South Asia DRF is most strongly influenced by foreign sources, and North America and Europe is the least. These rankings also reflect the strength of local emissions relative to world emissions, as discussed in section 2. Interestingly, RAIR values for AOD and DRF of sulfate (10-30%) are consistently smaller than that for aerosol column loading (i.e., 24-37%) [see Table 4.4 in HTAP 2010]. For POM, RAIR values (16-18%) for AOD and DRF in NA and EU are also somewhat smaller than the corresponding RAIR values (21-23%) for the column mass loading. These differences probably stem from transported sulfate and POM aerosols experiencing lower relative humidity at high altitude (resulting in lower optical depth) than local aerosols, which generally remain at lower altitudes. Finally, model variability is very large, highlighting the significant uncertainties in modeling aerosol processes.

The contributions of emission reductions in a receptor region depend on source regions. **Table 7** lists the response of annual mean AOD and all-sky DRF in receptor regions to a 20% reduction of anthropogenic emissions in the four source regions. Here we combine SO_4 and POM together, in which SO_4 makes a dominant contribution of 69-94%, depending on regions. BC is listed separately from the SO_4 and POM combined, because

strongly absorbing BC has different effects on solar radiation than do weakly absorbing sulfate and organic matter. Not surprisingly, the influences on AOD and DRF from the reduction of domestic emissions is about an order of magnitude larger than from any foreign source region. Foreign source regions also differ in contributing to the total import for a specific receptor region. The intercontinental transport of EA emissions accounts for the largest fraction of total import in NA, i.e., 60% and 70% for SO_4+POM, and BC, respectively. The NA emissions make the largest contribution (57%) to the total import of SO_4+POM into EU. For BC aerosols imported to EU, on the other hand, the EA contribution of 45% exceeds the NA contribution of 35%, presumably because of much higher BC emissions in EA. The imported BC to EA comes mostly (65%) from SA, followed by those from EU (e.g., 30%). For the import of SO_4+POM to EA, SA and EU emissions make quite comparable contributions, which is more than a factor of 3 larger than NA emissions. In SA, the imported SO_4+POM is significant, with RAIR of 24%, of which 66% comes from EU, followed by 28% from EA. For BC aerosols in SA, the import from EA and EU emissions contributes more or less equally (e.g., 48% and 44%).

Our multi-model estimates of the relative contributions of local emissions and ICT import are generally consistent with results in literature. In NA, we estimate that local emissions account for about 81% of anthropogenic AOD, which is higher than 66% estimated by a modeling study *[Leibensperger et al., 2012]*. This difference would be narrowed if emissions in regions other than the four defined regions of this study are taken into account. Yu et al. *[2012a]* estimate based on satellite measurements that the imported pollution via trans-Pacific transport results in a clear-sky TOA direct forcing of -0.49

443 Wm^{-2} over NA, which accounts for about 11.5% of total anthropogenic aerosol direct
444 forcing. For comparison, our estimated contribution by ICT import to the direct forcing
445 over NA is 14.7% in this study. The BC fractional contributions from different source
446 regions as estimated in this study also agree well with a model estimate [*Reddy and*
447 *Boucher, 2009*, referred to as RB09]. RB09 estimated that over North America, emissions
448 from East and South Asia contribute to 18% and 6% of the total BC burden, respectively,
449 which are somewhat smaller than our corresponding estimate of 23% and 8%. The
450 contribution of North America emissions to BC burden in Europe was estimated at 5% in
451 RB09, which is also somewhat smaller than our estimated 8%. RB09 estimated that the
452 local BC emissions over South and East Asia accounts for more than 80% of the BC
453 burden, which agrees well with our estimate of 82% and 84%. These comparisons show
454 how the estimated significance of ICT import in this study agrees broadly with results in
455 the literature, as these studies have defined source regions somewhat differently.
456

457 ## 4. Conclusions and discussion

458 We have assessed impacts of a 20% reduction of anthropogenic emissions in North
459 America, Europe, East Asia, and South Asia on the aerosol optical depth and direct
460 radiative forcing by using results from 10 global chemical transport models. On the basis
461 of the multi-model average, a 20% reduction of anthropogenic emissions in the four
462 regions combined lowers the global mean AOD and DRF by about 9%, 4%, and 10% for
463 sulfate, organic matter, and black carbon aerosol, respectively. Despite the considerable
464 model-to-model differences in the magnitude of forcing efficiency (direct radiative
465 forcing per unit emissions), the models appear to consistently give a lower sulfate forcing

466 efficiency for SO_2 emissions from EA than that from EU, and the largest BC forcing
467 efficiency for the EU emissions. These results may suggest that reducing BC emissions in
468 EU would be relatively the most efficient way to mitigate the warming effect of BC
469 aerosol, not considering cost and feasibility. However, a larger potential for BC
470 reductions is available in East Asia. Reducing SO_2 emissions decreases the cooling effect
471 of aerosols that counteracts the greenhouse warming; but the impact of reducing EA SO_2
472 is less pronounced (ca. 25%) than reducing EU, NA, or SA SO_2 by the same amount.
473 However, such implications need to be further explored by taking into account a variety
474 of aerosol impacts on climate through modifying cloud microphysics, changing
475 atmospheric circulations, and altering the snow albedo. The air quality implication of
476 any emission control should also be considered.
477
478 Our multi-model simulations of source-receptor relationships show that the impacts of
479 the regional emission reductions are not confined to the region itself because of aerosol
480 intercontinental transport. On an annual basis, intercontinental transport accounts for 10-
481 30% of the overall AOD or DRF in a receptor region, compared to the influence of both
482 regional emissions and intercontinental transport, depending on regions and species.
483 While South Asia is most influenced by import of sulfate aerosol from Europe, North
484 America is most influenced by import of black carbon aerosol from East Asia. Given that
485 BC deposition may accelerate the melting of snow in the Sierra Nevada and cause water
486 supply shortage in summer in the western U.S. *[Hadley et al., 2010]*, the region may
487 likely benefit from a future control of BC emissions in Asia.
488

The multi-model assessment shows large differences between models in the impacts of emission reductions and the role of intercontinental transport, which highlights a need for improving models and developing observational databases for evaluating and constraining models. Quantifying anthropogenic AOD distributions from satellite measurements remains challenging, in particular over land. Current estimates of anthropogenic AOD based on total AOD and fine-model fraction measurements from MODIS are only feasible over ocean and subject to large uncertainties *[Yu et al., 2009; Bellouin et al., 2005, 2008]*. Such an estimate would be better constrained by a synergistic use of aerosol microphysical measurements as provided by other satellite sensors *[Yu et al., 2012b* and references therein]. Large-scale in situ measurements of anthropogenic AOD will be essential for evaluating satellite observations and model simulations. From the perspective of model improvements, efforts should focus on not only emission inventories *[Textor et al., 2007]* but also a variety of atmospheric processes that determine the atmospheric evolution of aerosols, such as parameterization of dry deposition and wet scavenging *[Prospero et al., 2011]*. Given that the aerosol intercontinental transport and its influences involve a wide span of scales, it is necessary to develop modeling systems that link the local, regional, intercontinental, and global scales.

Acknowledgements: HY was supported by NASA grant NNX11AH66G, managed by Richard Eckman. MC and HB were supported by NASA Modeling, Analysis, and Prediction program managed by David Considine. NB thanks Shekar Reddy, formerly with the Met Office Hadley Centre, for carrying out the HadGEM2 simulations. We are

grateful to many colleagues, including Frank Dentener and Bill Collins for helpful comments. The HTAP experiments used in this study were organized by Martin Schultz, Arlene Fiore, Kees Cuvelier, Frank Dentener, Christiane Textor, Terry Keating, and Andre Zuber.

References

Albrecht, B. (1989), Aerosols, cloud microphysics, and fractional cloudiness, *Science*, **245**, 1227-1230.

Anderson, T.L., et al. (2005), An "A-Train" strategy for quantifying direct aerosol forcing of climate, *Bull. Am. Met. Soc.,* **86**, 1795-1809.

Bellouin, N., O. Boucher, J. Haywood, and M. S. Reddy (2005), Global estimate of aerosol direct radiative forcing from satellite measurements, *Nature*, **438**, 1138-1141, doi:10.1038/nature04348.

Bellouin, N., J. Rae, A. Jones, C. Johnson, J. Haywood, and O. Boucher (2011), Aerosol forcing in the Climate Model Intercomparison Project (CMIP5) simulations by HadGEM2-ES and the role of ammonium nitrate, *J. Geophys. Res.,* **116**, D20206, doi:10.1029/2011JD016074.

Bellouin, N., A. Jones, J. Haywood, and S. A. Christopher (2008), Updated estimate of aerosol direct radiative forcing from satellite observations and comparison against the Hadley Centre climate model, *J. Geophys. Res.*, **113**, D10205, doi:10.1029/2007JD009385.

Bian, H., M. Chin, J. M. Rodriguez, H. Yu, J. E. Penner, and S. Strahan (2009), Sensitivity of aerosol optical thickness and aerosol direct radiative effect to relative humidity, *Atmos. Chem. Phys.,* **9**, 2375-2386, doi:10.5194/acp-9-2375-2009.

CCSP (2009), Atmospheric Aerosol Properties and Climate Impacts, A Report by the *U.S. Climate Change Science Program and the Subcommittee on Global Change*

539 *Research*. [Mian Chin, Ralph A. Kahn, and Stephen E. Schwartz (eds.)]. National
540 Aeronautics and Space Administration, Washington, D.C., USA, 128 pp.
541 Chin, M., et al. (2002), Tropospheric aerosol optical thickness from the GOCART model
542 and comparisons with satellite and sun photometer measurements, *J. Atmos., Sci.,*
543 **59**, 461–483.
544 Chin, M., T. Diehl, P. Ginoux, and W. Malm (2007), Intercontinental transport of
545 pollution and dust aerosols: implications for regional air quality*, Atmos. Chem.*
546 *Phys.,* **7,** 5501-5517, doi:10.5194/acp-7-5501-2007.
547 Chin, M., T. Diehl, O. Dubovik, T. F. Eck, B. N. Holben, A. Sinyuk, and D. G. Streets
548 (2009), Light absorption by pollution, dust and biomass burning aerosols: A global
549 model study and evaluation with AERONET data. *Ann. Geophys.,* **27**, 3439-3464.
550 Chou, M. D., M. J. Suarez, C. H. Ho, M. M. H. Yan, and K. T. Lee (1998),
551 Parameterizations for cloud overlapping and shortwave single-scattering properties
552 in the Goddard GCM, *J. Climate,* **11**, 201–214.
553 Chung, S. H., and J. H. Seinfeld (2002), Global distribution and climate forcing of
554 carbonaceous aerosols, *J. Geophys. Res.*, **107**, 4407, doi:10.1029/2001JD001397.
555 Clarke, A., and V. Kapustin (2010), Hemispheric aerosol vertical profiles: Anthropogenic
556 impacts on optical depth and cloud nuclei, *Science*, **329**, 1488-1492.
557 Dirksen, R. J., K. F. Boersma, J. de Laat, P. Stammes, G. R. van der Werf, M. Val
558 Martin, and H. M. Kelder (2009), An aerosol boomerang: Rapid around-the-world
559 transport of smoke from the December 2006 Australian forest fires observed from
560 space, *J. Geophys. Res.,* **114**, D21201, doi:10.1029/2009JD012360.
561 Fiore, A. M., et al. (2009), Multimodel estimates of intercontinental source-receptor
562 relationships for ozone pollution, *J. Geophys. Res.*, **114**, D04301,
563 doi:10.1029/2008JD010816.
564 Fischer, E. V., D. A. Jaffe, N. A. Marley, J. S. Gaffney, and A. Marchany-Rivera (2010),
565 Optical properties of aged Asian aerosols observed over the U.S. Pacific Northwest,
566 *J. Geophys. Res.*, **115**, D20209, doi:10.1029/2010JD013943.
567 Forster, P., et al. (2007), Changes in Atmospheric Constituents and Radiative Forcing.
568 *Climate Change 2007: The Physical Scientific Basis*, Cambridge University Press,
569 United Kindom and New York, NY, USA.

570 Fry, M. M., et al. (2012), The influence of ozone precursor emissions from four world
571 regions on tropospheric composition and radiative climate forcing, *J. Geophys. Res.,*
572 **117**, D07306, doi:10.1029/2011JD017134.
573 Gunn, R., and B. B. Philips (1957), An experimental investigation of the effect of air
574 pollution on the initiation of rain, *J. Meteorol.,* **14**, 272-280.
575 Hadley, O. L., V. Ramanathan, G. R. Carmichael, Y. Tang, C. E. Corrigan, G. C.
576 Roberts, and G. S. Mauger (2007), Trans-Pacific transport of black carbon and fine
577 aerosols (D < 2.5 **μ**m) into North America, *J. Geophys. Res.,* **112**, D05309,
578 doi:10.1029/2006JD007632.
579 Hadley, O. L., C. E. Corrigan, T. W. Kirchstetter, S. Cliff, and V. Ramanathan, Measured
580 black carbon deposition on the Sierra Nevada snow pack and implication for snow
581 pack retreat. *Atmos. Chem. Phys*., **10,** 7505-7513, 2010.
582 Hauglustaine, D. A., F. Hourdin, S. Walters, L. Jourdain, M.-A. Filiberti, J.-F.
583 Larmarque, and E. A. Holland (2004), Interactive chemistry in the Laboratoire de
584 Météorologie Dynamique general circulation model: description and background
585 tropospheric chemistry evaluation, *J. Geophys. Res*., **109**, D04314,
586 doi:10.1029/3JD003957.
587 Heald, C. L., et al. (2006), Transpacific transport of Asian anthropogenic aerosols and its
588 impact on surface air quality in the United States, *J. Geophys. Res.*, **111**, D14310,
589 doi:10.1029/2005JD006847.
590 Hess, M., P. Koepke, and I. Schult (1998), Optical Properties of Aerosols and Clouds:
591 The Software Package OPAC, *Bull. Amer. Meteor. Soc.,* **79**, 831–844.
592 HTAP (2010), *Hemispheric Transport of Air Pollution 2010* - Part A: Ozone and
593 Particulate Matter, Air Pollution Studies No. 17, edited by Frank Dentener, terry
594 Keating, and Hajime Akimoto, United Nations, New York and Geneva.
595 Jacobson, M. Z. (2001), Strong radiative heating due to the mixing state of black carbon
596 in atmospheric aerosols, *Nature*, **409**, 695-697.
597 Kinne, S., et al. (2006), An AeroCom initial assessment – optical properties in aerosol
598 component modules of global models, *Atmos. Chem. Phys.*, **6**, 1815-1834,
599 doi:10.5194/acp-6-1815-2006.

600 Koch, D., G. A. Schmidt, and C. Field (2005), Sulfur, sea salt and radionuclide aerosols
601 in GISS, ModelE, *J. Geophys. Res.,* **111**, D06206, doi:10.1029/2004JD005550.
602 Koch, D., T. C. Bond, D. G. Streets, N. Unger, and G. R. van der Werf (2007), Global
603 impacts of aerosols from particular source regions and sectors, *J. Geophys. Res.*,
604 **112**, D02205, doi:10.1029/2005JD007024.
605 Leibensperger, E. M., et al. (2012), Climatic effects of 1950-2050 changes in US
606 anthropogeic aerosols – Part 1: Aerosol trends and radiative forcing, *Atmos. Chem.*
607 *Phys.*, **12**, 3333-3348.
608 Li, Z., K.-H. Lee, Y. Wang, J. Xin, and W.-M. Hao (2010), First observation-based
609 estimates of cloud-free aerosol radiative forcing across China, *J. Geophys. Res.*,
610 **115**, D00K18, doi:10.1029/2009JD013306.
611 McCormick, R. A., and J. H. Ludwig (1967), Climate modification by atmospheric
612 aerosols, *Science*, **156,** 1358-1359.
613 Pfister, G. G., P. G. Hess, L. K. Emmons, P. J. Rasch, and F. M. Vitt (2008), Impact of
614 the summer 2004 Alaska files on top of the atmosphere clear-sky radiation fluxes, *J.*
615 *Geophys. Res.*, **113**, D02204, doi:10.1029/2007JD008797.
616 Pozzoli, L, I. Bey, S. Rast, M. G. Schultz, P. Stier, and J. Feichter (2008a), Trace gas and
617 aerosol interactions in the fully coupled model of aerosol-chemistry-climate
618 ECHAM5-HAMMOZ: 1. Model description and insights from the spring 2001
619 TRACE-P experiment, *J. Geophys. Res.,* **113**, D07308,
620 doi:10.1029/2007/JD009007.
621 Pozzoli, L, I. Bey, S. Rast, M. G. Schultz, P. Stier, and J. Feichter (2008b), Trace gas and
622 aerosol interactions in the fully coupled model of aerosol-chemistry-climate
623 ECHAM5-HAMMOZ: 2. Impact of heterogeneous chemistry on the global aerosol
624 distribution, *J. Geophys. Res.,* **113**, D07309, doi:10.1029/2007/JD009008.
625 Prospero, J. M., D. L. Savoie, and R. Arimoto (2003), Long-term record of nss-sulfate
626 and nitrate in aerosols on Midway Island, 1981-2000: Evidence of increased (now
627 decreasing?) anthropogenic emissions from Asia, *J. Geophys. Res.,* **108**, 4019,
628 doi:10.1029/2001JD001524.

629 Prospero, J. M., W. M. Landing, and M. Schulz (2010), African dust deposition to
630 Florida: Temporal and spatial variability and comparisons to models, *J. Geophys.*
631 *Res.,* **115**, D13304, 10.1029/2009jd012773.
632 Ramanathan, V., et al. (2001), Indian Ocean Experiment: An integrated analysis of the
633 climate forcing and effects of the great Indo-Asian haze, *J. Geophys. Res.*, **106**,
634 28,371–28,398, doi:10.1029/2001JD900133.
635 Ramanathan, V., et al. (2007), Atmospheric brown clouds: Hemispherical and regional
636 variations in long-range transport, absorption, and radiative forcing, *J. Geophys.*
637 *Res.*, **112**, D22S21, doi:10.1029/2006JD008124.
638 Reddy, M. S., and O. Boucher (2009), Climate impacts of black carbon emitted from
639 energy consumption in the world's regions. *Geophys. Res. Lett.*, **34**, L11802,
640 doi:10.1029/2006GL028904.
641 Rotman, D. A., et al. (2004), IMPACT, the LLNL 3-D global atmospheric chemical
642 transport model for the combined troposphere and stratosphere: Model description
643 and analysis of ozone and other trace gases, *J. Geophys. Res.,* **109**, D04303,
644 doi:10.1029/2002JD003155.
645 Rudich, Y., Y. J. Kaufman, U. Dayan, H. Yu, and R. G. Kleidman (2008), Estimation of
646 transboundary transport of pollution aerosols by remote sensing in the eastern
647 Mediterranean, *J. Geophys. Res.*, **113**, D14S13, doi:10.1029/2007JD009601.
648 Satheesh, S. K., and V. Ramanathan (2000), Large differences in tropical aerosol forcing
649 at the top of atmosphere and Earth's surface, *Nature*, **405**, 60-63.
650 Schulz, M., et al. (2006), Radiative forcing by aerosols as derived from the AeroCom
651 present-day and pre-industrial simulations, *Atmos. Chem. Phys.,* **6**, 5225-5246,
652 doi:10.5194/acp-6-5225-2006.
653 Schulz, M. (2007), Constraining model estimates of the aerosol radiative forcing, Thèse
654 d'Habilitation à Diriger des Recherches, Université Pierre et Marie Curie, Paris
655 VI .
656 Shindell, D. T., et al. (2006), Simulations of preindustrial, present-day, and 2100
657 conditions in the NASA GISS composition and climate model G-PUCCINI, *Atmos.*
658 *Chem. Phys.,* **6**, 4427-4459, doi:10.5194/acp-6-4427-2006.

659 Shindell, D., et al. (2008a), Climate forcing and air quality change due to regional
660 emissions reductions by economic sector, *Atmos. Chem. Phys.*, **8**, 7101-7113.
661 Shindell, D., et al. (2008b), Multimodel projections of climate change from short-lived
662 emissions due to human activities. *J. Geophys. Res.,* **113**, D11109,
663 doi:10.1029/2007JD009152.
664 Shindell, D., et al. (2008c), A multi-model assessment of pollution transport to the Arctic.
665 *Atmos. Chem. Phys.,* **8**, 5353-5372.
666 Takemura, T., T. Nozawa, S. Emori, T. Y. Nakajima, and T. Nakajima (2005),
667 Simulation of climate response to aerosol direct and indirect effects with aerosol
668 transport-radiation model. *J. Geophys. Res.*, **110**, D02202,
669 doi:10.1029/2004JD005029.
670 Textor, C., et al. (2006), Analysis and quantification of the diversities of aerosol life
671 cycles within AeroCom, *Atmos. Chem. Phys.,* **6**, 1777-1813, doi:10.5194/acp-6-
672 1777-2006.
673 Textor, C., et al. (2007), The effect of harmonized emissions on aerosol properties in
674 global models – an AeroCom experiment, *Atmos. Chem. Phys.*, **7**, 4489-4501.
675 Twomey, S. (1977), The influence of pollution on the shortwave albedo of clouds, *J.*
676 *Atmos. Sci.,* **34**, 1149-1152.
677 VanCuren, R. A. (2003), Asian aerosols in North America: Extracting the chemical
678 composition and mass concentration of the Asian continental aerosol plume from
679 long-term aerosol records in the western United States, *J. Geophys. Res.,* **108**, 4623,
680 doi:10.1029/2003JD003459.
681 Yu, H., et al. (2004), The direct radiative effect of aerosols as determined from a
682 combination of MODIS retrievals and GOCART simulations, *J. Geophys. Res*., **109**,
683 D03206, doi:10.1029/2003JD003914.
684 Yu, H., et al. (2006), A review of measurement-based assessments of the aerosol direct
685 radiative effect and forcing, *Atmos. Chem. Phys*., **6**, 613-666, doi:10.5194/acp-6-
686 613-2006.
687 Yu, H., L. A. Remer, M. Chin, H. Bian, R. G. Kleidman, and T. Diehl (2008), A satellite-
688 based assessment of transpacific transport of pollution aerosol, *J. Geophys. Res.,*
689 **113**, D14S12, doi:10.1029/2007JD009349.

690 Yu, H., M. Chin, L. A. Remer, R. G. Kleidman, N. Bellouin, H. Bian, and T. Diehl
691 (2009), Variability of marine aerosol fine-mode fraction and estimates of
692 anthropogenic aerosol component over cloud-free oceans from the Moderate
693 resolution Imaging Spectroradiometer (MODIS), *J. Geophys. Res.*, **114**,
694 D10206,10.1029/2008JD010648.
695 Yu, H., L. A. Remer, M. Chin, H. Bian, Q. Tan, T. Yuan, and Y. Zhang (2012a),
696 Aerosols from overseas rival domestic emissions over North America, submitted to
697 *Science*.
698 Yu, H., et al. (2012b), Satellite perspective of aerosol intercontinental transport,
699 submitted to *Atmos. Res.*
700 Zhou, M., H. Yu, R. E. Dickinson, O. Dubovik, and B. N. Holben (2005), A normalized
701 description of the direct effect of key aerosol types on solar radiation as estimated
702 from AERONET aerosols and MODIS albedos. *J. Geophys. Res.*, **110**, D19202,
703 10.1029/2005JD005909.
704

Table Captions

Table 1. List of 10 models that participated in HTAP aerosol S/R experiments and are used in this analysis.

Table 2. Comparisons of AOD at 550 nm (τ) from 9 HTAP models in this study with that inferred from Schulz et al. (2006). For SO_4 and POM, AOD is inferred by using anthropogenic AOD and anthropogenic fraction of present day AOD. For BC, we infer AOD from the anthropogenic absorptive AOD reported in Schulz et al. *[2006]* by assuming that all BC is anthropogenic and BC has a single scattering albedo of 0.2 at 550 nm.

Table 3. Annual mean aerosol direct radiative forcing normalized by AOD at 550 nm (NDRF, $Wm^{-2}\tau^{-1}$) at top of atmosphere (TOA) and surface for SO_4, POM, and BC) in the four source regions (NA, EU, EA, SA) and globe, which is derived from GOCART simulated monthly AOD and DRF for 2001.

Table 4. Change of global annual mean AOD (τ x 1000, mean ± std. dev) in response to the 20% reduction of anthropogenic emissions in 4 source regions (SR6 - SR1) of 9 HTAP models.

Table 5. Change of global annual mean aerosol DRF (unit: mWm^{-2}, mean ± standard deviation, 1 mWm^{-2} = 0.001 Wm^{-2}) in response to the 20% reduction of anthropogenic emissions in 4 source regions as derived from analysis of SR1 and SR6 runs of 9 HTAP models.

Table 6. Global annual average TOA all-sky forcing efficiency relative to emissions from the source regions (unit: mWm^{-2} per Tg) as derived from 8 HTAP models. The forcing efficiency for SO_4 and POM is calculated with respect to SO_2 and primary POM emissions, although some models with fully coupled chemistry include changes of SO_4 resulting from the reductions of other emissions and a fraction of POM is secondary aerosol produced from a variety of volatile organic carbon.

737

738 **Table 7**: Response of annual AOD and all-sky DRF (mean ± std. dev.) in the receptor regions
739 (columns) to 20% reductions of anthropogenic gas and aerosol emissions in the source regions
740 (rows) estimated from 9 HTAP models. Percentage contributions of individual source regions
741 are shown in parentheses for AOD (corresponding percentages for DRF are only slightly
742 different and hence not shown). Contributions of a region on itself (termed "domestic") are
743 shown in bold. Here BC is listed separately from SO_4 and POM combined (in which SO_4
744 makes a dominant contribution of 69-94%, depending on region), because of their distinct
745 effects on solar radiation. For SO_4+POM, surface DRF is slightly greater than TOA DRF
746 because of weak absorption and not shown. A positive change of DRF for SO_4+POM suggests
747 a weakened cooling effect by the emission reduction. A BC emission reduction introduces a
748 negative change of TOA DRF (a weakened warming effect) and a positive change of surface
749 DRF (a weakened cooling effect).

750

751

Figure Captions

Figure 1: Illustration of four HTAP defined regions for examining the source-receptor relationships for anthropogenic aerosols: North America (NA, 15°-55°N, 60°W-125°W), Europe (EU, 25°-65°N, 10°W-50°E), East Asia (EA, 15°-50°N, 95°-160°E), and South Asia (SA, 5°-35°N, 50°-95°E). Regional and annual anthropogenic emissions of SO_2, primary POM, and BC from 8 HTAP models (excluding HADGEM2 and ECHAM5) are shown in bar charts, with error bar indicating the range of 8 models.

Figure 2: Annual average AOD for the external mixture of sulfate, POM, and BC simulated by baseline runs of 9 HTAP models.

Figure 3: Comparison of HTAP SR1 9-model median AOD for the external mixture of sulfate, POM, and BC (a) with MODIS-derived anthropogenic AOD over ocean as described in Yu et al. *[2009]* (b) and Bellouin et al. *[2008]* (c).

Figure 4: Comparisons of zonal variations of seasonal and 20°N-60°N average AOD for sulfate, POM, and BC combined as simulated by HTAP models (black line for median and shaded area for the range of 9 HTAP models) with the MODIS-derived over-ocean anthropogenic AOD (red line for *Yu et al., 2009* and blue line for *Bellouin et al., 2008*).

Figure 5: Seasonal variations of 9-model average TOA DRF (a), and surface DRF (b) in all-sky conditions (Wm^{-2}) for the external mixture of sulfate, POM, and BC as derived from the HTAP baseline simulations (SR1).

Figure 6: Global annual mean forcing efficiency (unit: mWm^{-2} per Tg) for sulfate (a) and BC (b) with respect to regional (denoted as NA, EU, EA, and SA) emissions as simulated by 8 HTAP models.

Figure 7: Annual average AOD (x100, top panel) and DRF (mWm^{-2}) at the top of atmosphere (TOA) (middle panel) and at the surface (bottom panel) in all-sky conditions resulting from 20% reductions of regional anthropogenic emissions over North America (NA), Europe (EU), East Asia (EA), and South Asia (SA), respectively. A positive value for DRF represents the reduced aerosol direct radiative forcing resulting from the reduction of emissions. Each of the four source regions is overlaid on corresponding SR6xx-SR1 maps where xx represents NA, EU, EA, and SA. Individual aerosol components are assumed to be mixed externally. The results are based on 9 HTAP models.

Figure 8: Seasonal variations of changes in the all-sky DRF (mWm^{-2}) at surface (SR6-SR1) due to 20% reduction of regional anthropogenic emissions derived from 9 HTAP models. Each of the four source regions is overlaid on corresponding SR6xx-SR1 maps where xx represents NA, EU, EA, and SA.

Figure 9: Ten-model (including ECHAM5) derived average relative annual intercontinental response (RAIR) for aerosol optical depth (AOD) in four receptor regions, by chemical component. Standard deviations, as indicated by error bars, reflect the model variability in simulating aerosol transport.

Figure 10: same as Figure 9 but for TOA all-sky DRF.

807

Table 1. List of 10 models that participated in HTAP aerosol S/R experiments and are used in this analysis

Model	Model version	Investigator(s)	Resolution (lon. x lat.)	Major Reference(s)
CAM-CHEM	v3311m13	P. Hess	2.5°x1.875°	*Pfister et al., 2008*
CAM-CHEM	v3514			
ECHAM5 HAMMOZ	v21	I. Bey, G. Forberth	2.813°x2.813°	*Pozzoli et al., 2008a and 2008b*
GISS PUCCINI	modelEaer	D. Shindell	5°x4°	*Koch et al., 2005; Shindell et al., 2006*
GMI	v02a	H. Bian	2.5°x2°	*Bian et al., 2009*
GOCART	v4p2	M. Chin, T. Diehl	2.5°x2°	*Chin et al., 2002, 2007, 2009*
HADGEM2	A-v01	N. Bellouin	1.875°x1.25°	*Bellouin et al., 2011*
INCA	v2	M. Schulz	3.75°x2.5°	*Schulz, 2007; Hauglustaine et al., 2004; Textor et al., 2006*
LLNL IMPACT	T5a	D. Bergmann, C. S. Atherton	2.5°x2°	*Rotman et al., 2004.*
SPRINTARS	v356	T. Takemura	1.125°x1.125°	*Takemura et al., 2005*

Acronyms for model names:

CAM-CHEM: Community Atmospheric Model – Chemistry version (NCAR, USA)
ECHAM5-HAMMOZ: Max-Planck Institute for Meteorology Hamburg Climate Model - version 5 with Hamburg Aerosol Model and MOZart chemistry sub-Module
GISS PUCCINI: Goddard Institute for Space Studies, Physical Understanding of Composition-Climate INteractions and Impacts model (NASA GISS, USA)
GMI: Global Modeling Initiative (NASA GSFC, USA)
GOCART: Goddard Chemistry Aerosol Radiation and Transport (NASA GSFC, USA)
HADGEM2: Hadley Centre Global Environment Model version 2 (Met Office, UK)
INCA: Interaction of Chemistry and Aerosol (laboratoire des Sciences du Climat et de l'Environnement, France)
LLNL IMPACT: Integrated Massively Parallel Atmospheric Chemical Transport model (Lawrence Livermore National Laboratory, USA)
SPRINTARS: Spectral Radiation-Transport Model for Aerosol Species (Kyushu University, Japan)

808

809

Table 2. Comparisons of AOD at 550 nm (τ) from 9 HTAP models in this study with that inferred from Schulz et al. (2006). For SO_4 and POM, AOD is inferred by using anthropogenic AOD and anthropogenic fraction of present day AOD. For BC, we infer AOD from the anthropogenic absorptive AOD reported in Schulz et al. *[2006]* by assuming that all BC is anthropogenic and BC has a single scattering albedo of 0.2 at 550 nm.

	This study	Schulz et al. *[2006]*
τ_{SO4}	0.0335 ± 0.0134	0.0345 ± 0.0164
τ_{POM}	0.0108 ± 0.0047	0.0151 ± 0.0094
τ_{BC}	0.0022 ± 0.0010	0.0024 ± 0.0010

810
811

812

Table 3. Annual mean aerosol direct radiative forcing normalized by AOD at 550 nm (NDRF, $Wm^{-2}\tau^{-1}$) at top of atmosphere (TOA) and surface for SO_4, POM, and BC) in the four source regions (NA, EU, EA, SA) and globe, which is derived from GOCART simulated monthly AOD and DRF for 2001.

Sky Condition	Region	$NDRF_{SO4}$		$NDRF_{POM}$		$NDRF_{BC}$	
		TOA	Surface	TOA	Surface	TOA	surface
All Sky	NA	-24.9	-24.5	-28.4	-39.1	84.6	-225.2
	EU	-21.1	-20.4	-22.6	-32.8	93.0	-190.8
	EA	-21.4	-21.2	-25.4	-35.1	83.2	-210.0
	SA	-24.9	-25.1	-28.7	-41.0	89.6	-235.2
	globe	-24.2	-24.1	-30.0	-41.5	85.9	-231.6
Clear Sky	NA	-30.6	-30.1	-35.4	-45.9	62.1	-246.1
	EU	-25.6	-24.6	-27.9	-37.9	80.2	-207.8
	EA	-26.6	-26.3	-32.1	-41.5	59.9	-231.3
	SA	-27.7	-27.8	-32.7	-44.8	74.6	-247.6
	globe	-30.2	-29.9	-37.0	-48.4	62.8	-252.7

813
814
815

816

Table 4. Change of global annual mean AOD (τ x 1000, mean ± std. dev) in response to the 20% reduction of anthropogenic emissions in 4 source regions (SR6 - SR1) of 9 HTAP models.

Source Region	τ_{SO4}	τ_{POM}	τ_{BC}	$\tau_{SO4+POM+BC}$
NA	-0.67 ± 0.23	-0.054 ± 0.036	-0.026 ± 0.013	-0.75 ± 0.23
EU	-1.13 ± 0.47	-0.084 ± 0.058	-0.050 ± 0.021	-1.28 ± 0.45
EA	-0.97 ± 0.38	-0.142 ± 0.101	-0.086 ± 0.047	-1.19 ± 0.37
SA	-0.32 ± 0.11	-0.102 ± 0.059	-0.038 ± 0.019	-0.46 ± 0.10
Total	-3.10 ± 1.11	-0.383 ± 0.246	-0.199 ± 0.093	-3.70 ± 1.08

817
818

819

Table 5. Change of global annual mean aerosol DRF (unit: mWm^{-2}, mean ± standard deviation, 1 mWm^{-2} = 0.001 Wm^{-2}) in response to the 20% reduction of anthropogenic emissions in 4 source regions as derived from analysis of SR1 and SR6 runs of 9 HTAP models.

Source Region	DRF_{SO4}	DRF_{POM}	DRF_{BC}	$DRF_{SO4+POM+BC}$
All-sky TOA DRF (mWm^{-2})				
NA	15.4 ± 5.1	1.4 ± 0.9	-3.0 ± 1.6	13.8 ± 5.3
EU	24.4 ± 8.9	1.6 ± 1.2	-5.9 ± 2.6	20.2 ± 9.5
EA	19.4 ± 7.9	3.1 ± 2.2	-9.4 ± 6.1	13.0± 9.9
SA	6.8 ± 1.9	2.5 ± 1.7	-3.6 ± 1.8	5.7 ± 2.6
Total	66.1 ± 22.8	8.6 ± 5.7	-21.9 ± 11.5	52.8 ± 25.3
All-sky surface DRF (mWm^{-2})				
NA	14.9 ± 4.9	1.9 ± 1.3	5.5 ± 2.4	22.4± 5.5
EU	23.0 ± 8.0	2.4 ± 1.7	8.8 ± 3.1	34.1 ± 7.3
EA	18.9 ± 7.5	4.4 ± 3.2	16.5 ± 8.7	39.9 ± 11.7
SA	6.9 ± 2.0	3.6 ± 2.3	8.1 ± 3.6	18.6 ± 4.6
Total	63.7 ± 21.4	12.3 ± 8.1	39.0 ± 16.6	115.0 ± 26.0

820
821
822

823

Table 6. Global annual average TOA all-sky forcing efficiency relative to emissions from the source regions (unit: mWm^{-2} per Tg) as derived from 8 HTAP models. The forcing efficiency for SO_4 and POM is calculated with respect to SO_2 and primary POM emissions, although some models with fully coupled chemistry include changes of SO_4 resulting from the reductions of other emissions and a fraction of POM is secondary aerosol produced from a variety of volatile organic carbon.

Source Region	SO_4	POM	BC
NA	-3.6±1.0	-4.3±1.5	27.2±14.2
EU	-3.7±1.1	-4.2±1.6	36.7±18.0
EA	-2.7±0.9	-3.6±1.7	27.7±19.0
SA	-3.8±1.0	-4.0±1.7	25.0±13.6
Total	-3.3±0.9	-3.9±1.6	29.0±16.8

824
825

826

Table 7: Response of annual AOD and all-sky DRF (mean ± std. dev.) in the receptor regions (columns) to 20% reductions of anthropogenic gas and aerosol emissions in the source regions (rows) estimated from 9 HTAP models. Percentage contributions of individual source regions are shown in parentheses for AOD (corresponding percentages for DRF are only slightly different and hence not shown). Contributions of a region on itself (termed "domestic") are shown in bold. Here BC is listed separately from SO_4 and POM combined (in which SO_4 makes a dominant contribution of 69-94%, depending on region), because of their distinct effects on solar radiation. For SO_4+POM, surface DRF is slightly greater than TOA DRF because of weak absorption and not shown. A positive change of DRF for SO_4+POM suggests a weakened cooling effect by the emission reduction. A BC emission reduction introduces a negative change of TOA DRF (a weakened warming effect) and a positive change of surface DRF (a weakened cooling effect).

	Receptor Region			
Source Region	NA	EU	EA	SA
SO_4+POM AOD (x1000)				
NA	**-8.53±2.85 (82%)**	-1.22±0.66 (7%)	-0.35±0.25 (2%)	-0.24±0.22 (2%)
EU	-0.42±0.21 (4%)	**-13.81±4.43 (84%)**	-1.21±0.68 (6%)	-2.18±0.79 (16%)
EA	-0.92±0.59 (9%)	-0.65±0.48 (4%)	**-16.42±5.02 (84%)**	-1.05±0.66 (8%)
SA	-0.54±0.91 (5%)	-0.72±1.32 (4%)	-1.68±0.95 (9%)	**-10.37±3.21 (75%)**
BC AOD (x1000)				
NA	**-0.28±0.09 (65%)**	-0.05±0.04 (8%)	-0.02±0.01 (1%)	-0.01±0.01 (1%)
EU	-0.02±0.02 (4%)	**-0.51±0.15 (76%)**	-0.05±0.03 (4%)	-0.08±0.04 (8%)
EA	-0.10±0.09 (23%)	-0.07±0.08 (10%)	**-1.04±0.28 (84%)**	-0.09±0.06 (9%)
SA	-0.04±0.03 (8%)	-0.04±0.03 (6%)	-0.14±0.08 (11%)	**-0.87±0.36 (82%)**
SO_4+POM all-sky TOA DRF (mWm^{-2})				
NA	**207.7±68.9**	28.8±14.9	7.5±5.2	6.3±5.7
EU	10.4±5.42	**304.4±93.3**	25.4±14.1	54.2±20.3
EA	23.8±15.1	14.4±10.9	**315.2±98.8**	25.0±15.5
SA	11.2± 15.5	8.8±9.4	32.9±15.4	**256.4±80.4**
BC all-sky TOA DRF (mWm^{-2})				
NA	**-23.8±7.2**	-5.1±3.3	-1.4±1.3	-1.5±1.3
EU	-1.7±1.4	**-45.6±12.8**	-4.5±2.7	-9.2±4.4
EA	-9.0±8.5	-6.7±7.3	**-83.5±22.3**	-8.6±6.5
SA	-3.0±2.3	-4.1±2.7	-11.8±5.3	**-70.7±29.6**
BC all-sky surface DRF (mWm^{-2})				
NA	**64.1±20.5**	11.5±7.2	3.3±3.0	3.5±2.8
EU	4.3±3.5	**103.0±27.1**	10.0±5.9	19.8±9.9
EA	22.7±21.6	14.4±15.5	**212.8±57.0**	22.3±15.0
SA	7.9±6.2	7.5±5.3	29.3±13.5	**202.0±85.4**

827

828

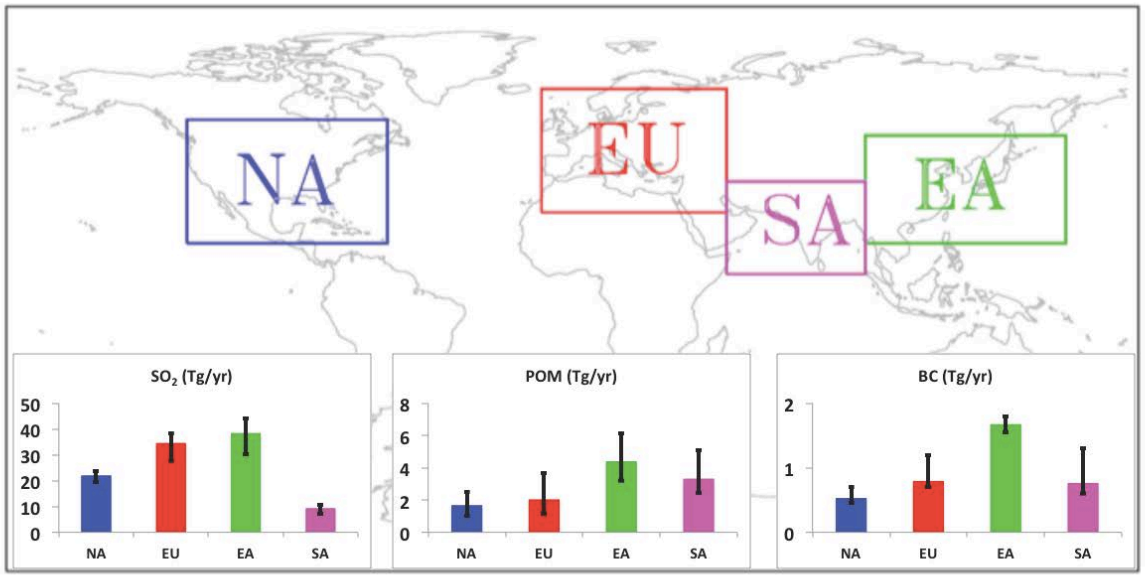

Figure 1: Illustration of four HTAP defined regions for examining the source-receptor relationships for anthropogenic aerosols: North America (NA, 15°-55°N, 60°W-125°W), Europe (EU, 25°-65°N, 10°W-50°E), East Asia (EA, 15°-50°N, 95°-160°E), and South Asia (SA, 5°-35°N, 50°-95°E). Regional and annual anthropogenic emissions of SO_2, primary POM, and BC from 8 models (excluding HADGEM2 and ECHAM5) are shown in bar charts, with error bar indicating the range of 8 models.

829
830
831

832

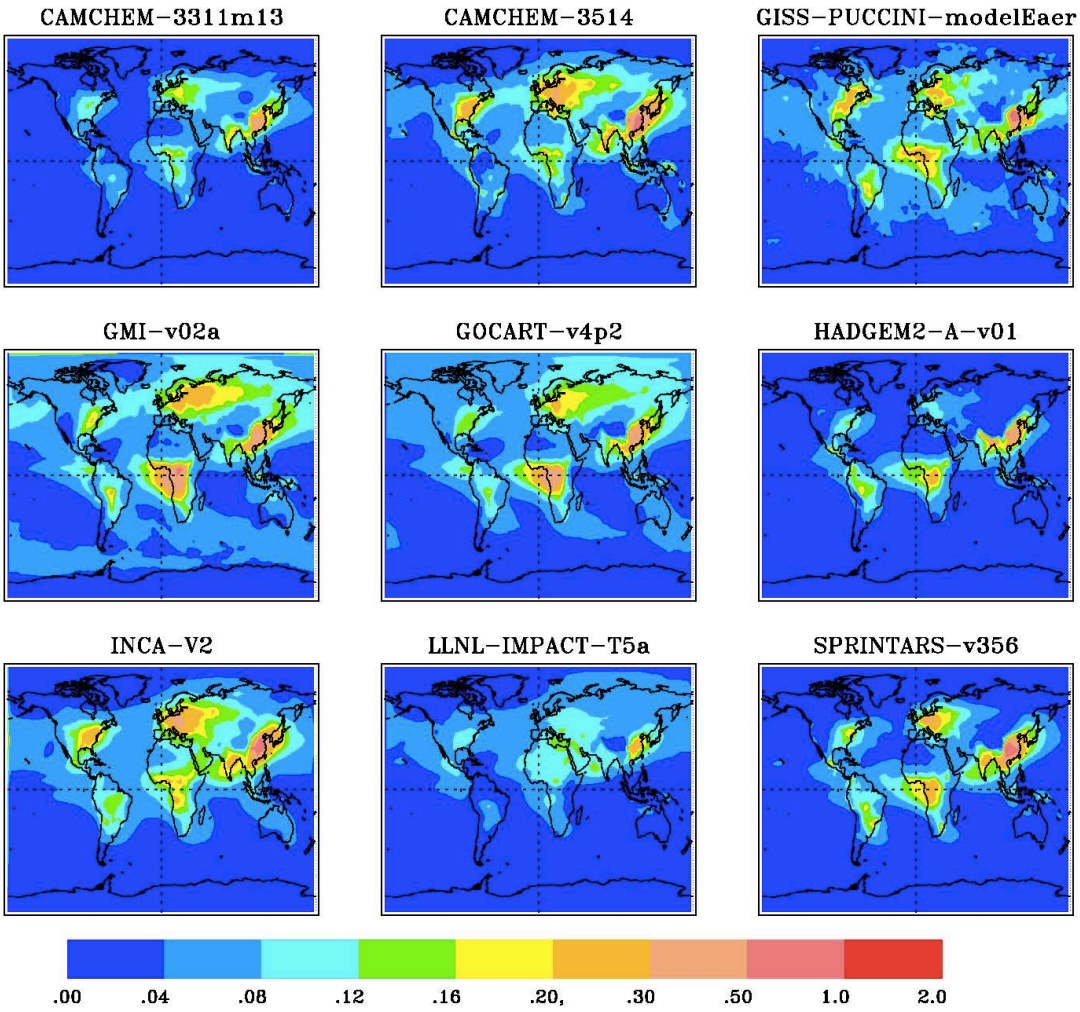

Figure 2: Annual average AOD for the external mixture of sulfate, POM, and BC simulated by baseline runs of 9 HTAP models.

833
834

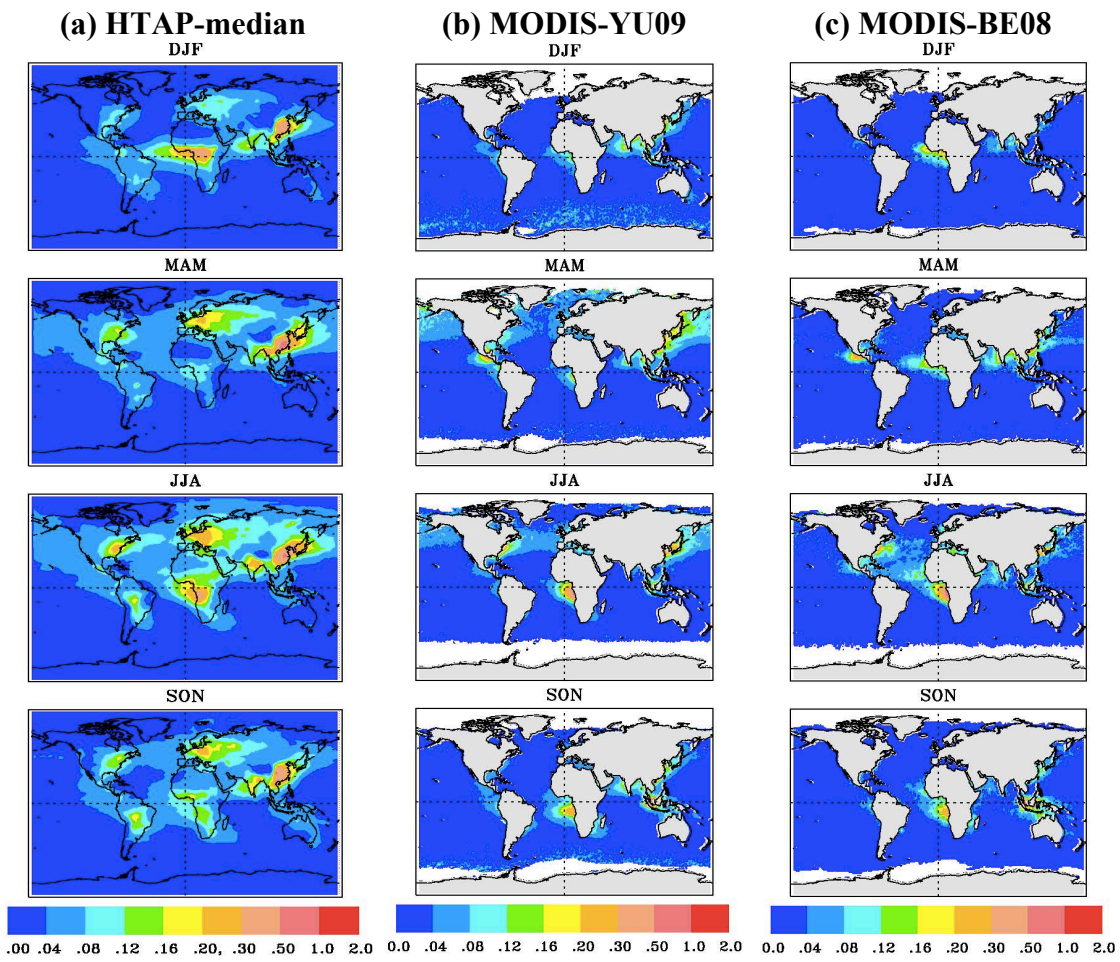

Figure 3: Comparison of HTAP SR1 9-model median AOD for the external mixture of sulfate, POM, and BC (a) with MODIS-derived anthropogenic AOD over ocean as described in Yu et al. *[2009]* (b) and Bellouin et al. *[2008]* (c).

844

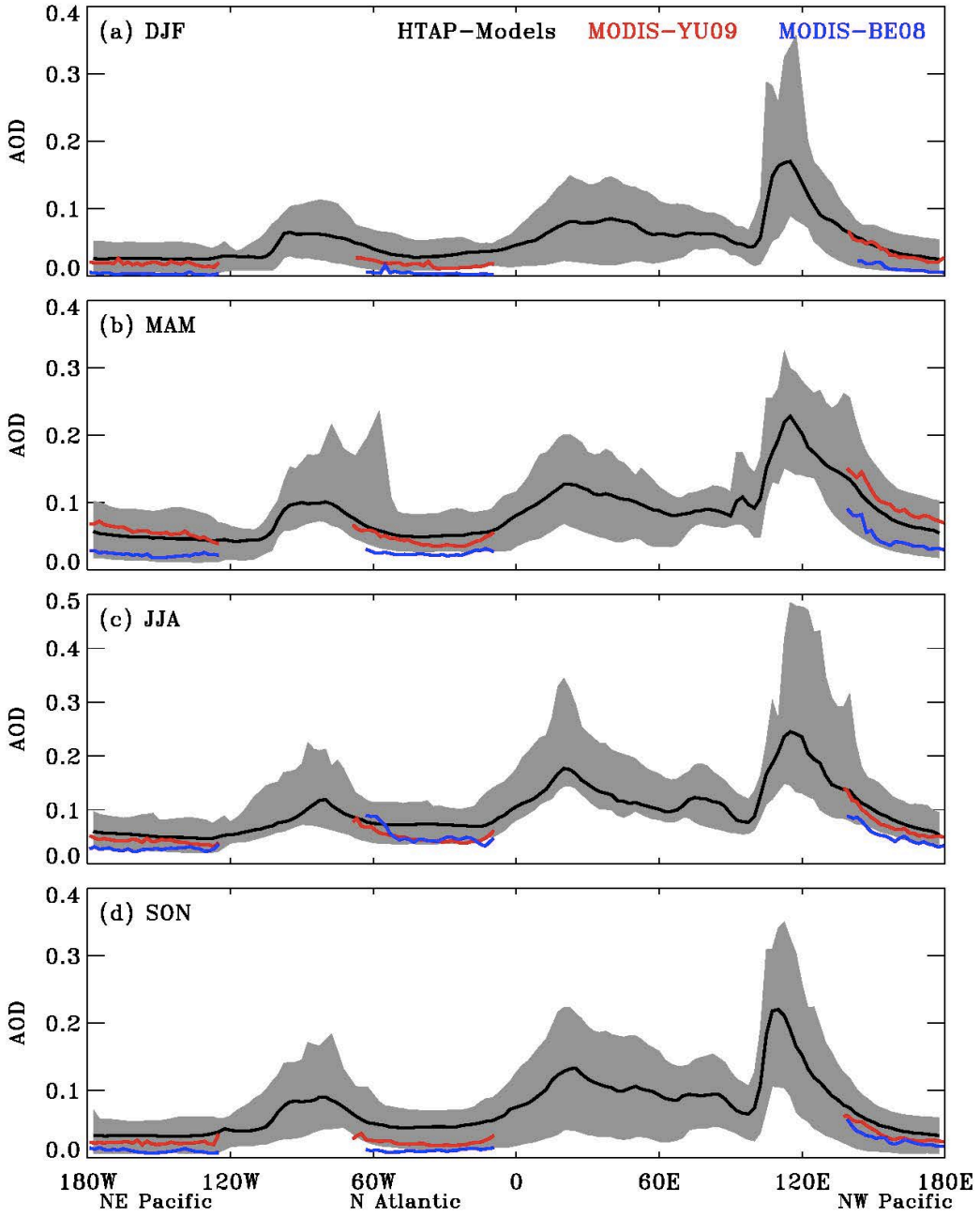

Figure 4: Comparisons of zonal variations of seasonal and 20°N-60°N average AOD for sulfate, POM, and BC combined as simulated by HTAP models (black line for median and shaded area for the range of 9 models) with the MODIS-derived over-ocean anthropogenic AOD (red line for *Yu et al., 2009* and blue line for *Bellouin et al., 2008*). Note that HTAP model results cover both land and ocean, while MODIS-based anthropogenic AOD were estimated only over ocean.

845

846

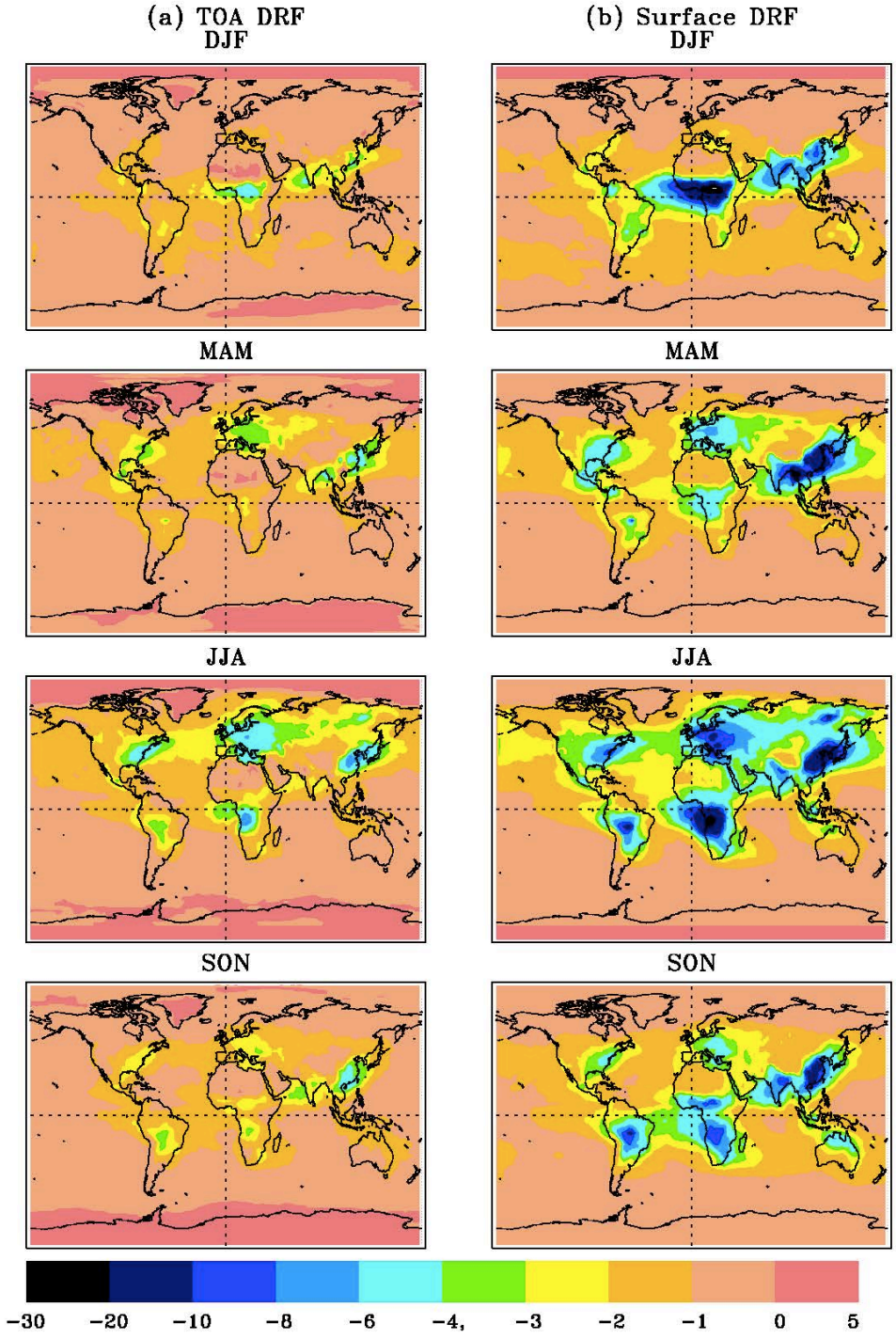

Figure 5: Seasonal variations of 9-model average TOA DRF (a), and surface DRF (b) in all-sky conditions (Wm^{-2}) for the external mixture of sulfate, POM, and BC as derived from the HTAP baseline simulations (SR1).

847

848
849

(a) Sulfate

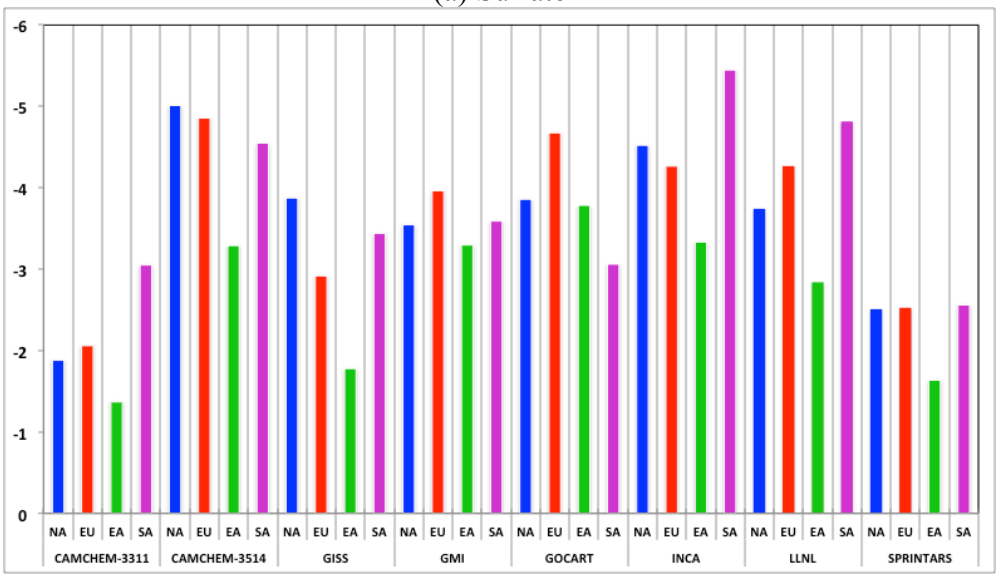

(b) BC

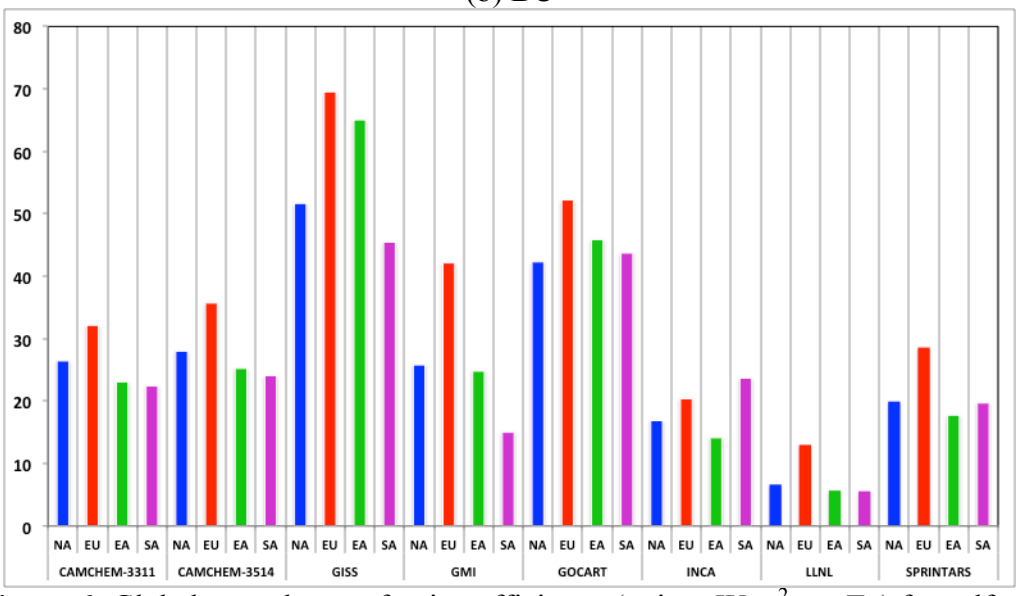

Figure 6: Global annual mean forcing efficiency (unit: mWm^{-2} per Tg) for sulfate (a) and BC (b) with respect to regional (denoted as NA, EU, EA, and SA) emissions as simulated by 8 HTAP models.

850
851

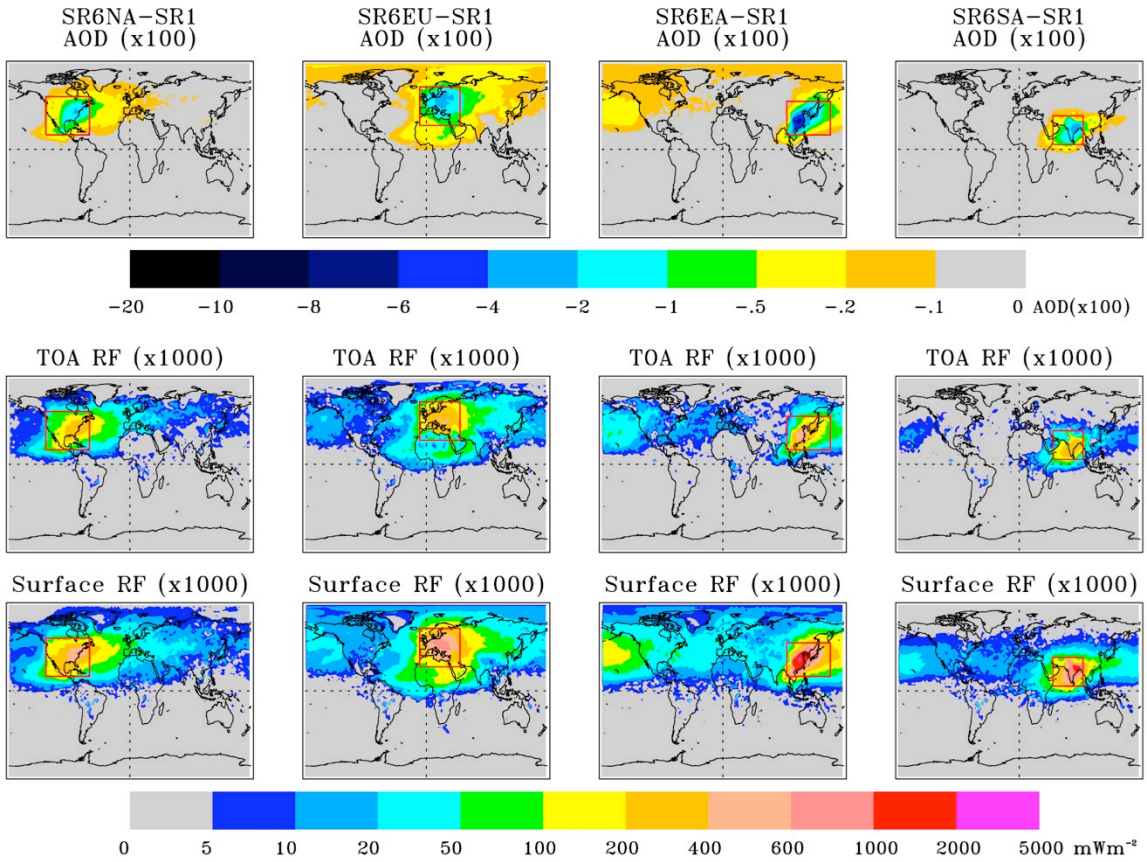

Figure 7: Annual average AOD (x100, top panel) and DRF (mWm^{-2}) at the top of atmosphere (TOA) (middle panel) and at the surface (bottom panel) in all-sky conditions resulting from 20% reductions of regional anthropogenic emissions over North America (NA), Europe (EU), East Asia (EA), and South Asia (SA), respectively. A positive value for DRF represents the reduced aerosol direct radiative forcing resulting from the reduction of emissions. Each of the four source regions is overlaid on corresponding SR6xx-SR1 maps where xx represents NA, EU, EA, and SA. Individual aerosol components are assumed to be mixed externally. The results are based on 9 HTAP models.

852

853

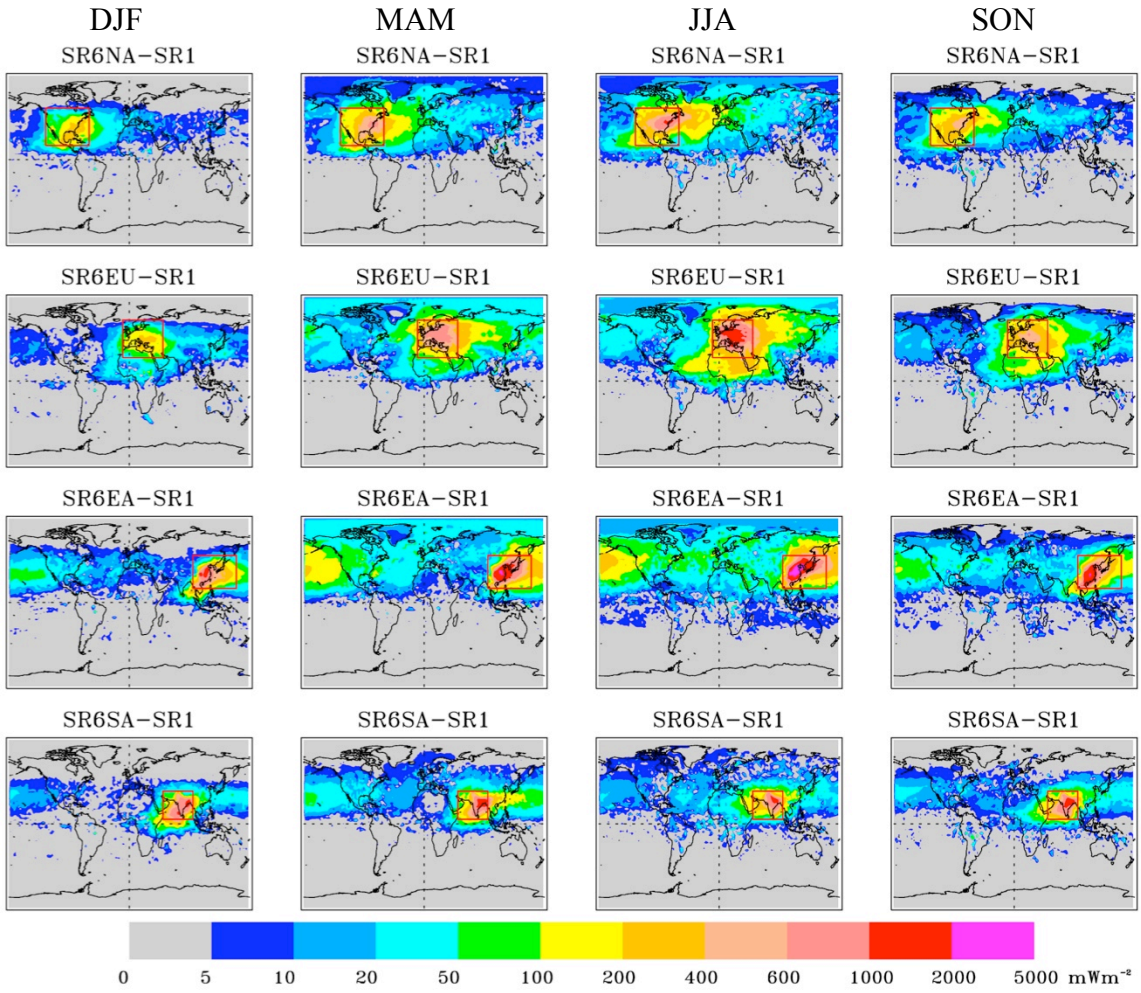

Figure 8: Seasonal variations of changes in the all-sky DRF (mWm^{-2}) at surface (SR6-SR1) due to 20% reduction of regional anthropogenic emissions derived from 9 HTAP models. Each of the four source regions is overlaid on corresponding SR6xx-SR1 maps where xx represents NA, EU, EA, and SA.

854

855

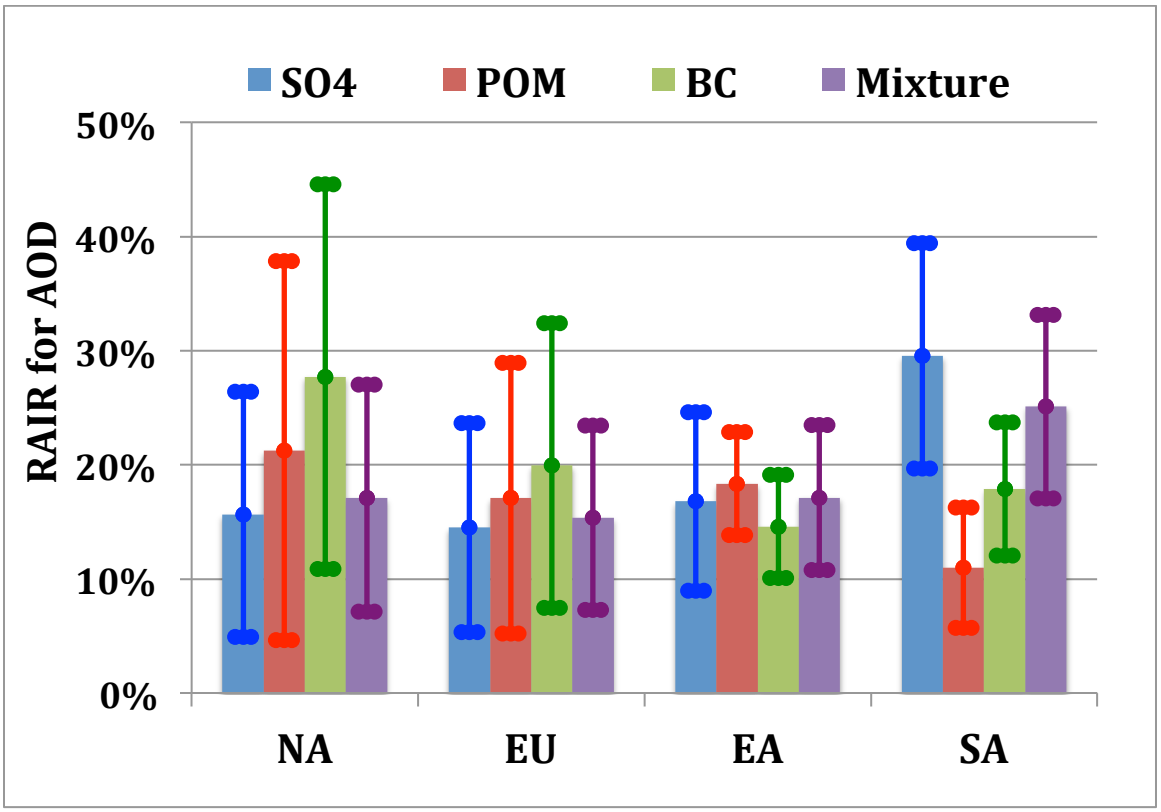

Figure 9: Ten-model (including ECHAM5) derived average relative annual intercontinental response (RAIR) for aerosol optical depth (AOD) in four receptor regions, by chemical component. Standard deviations, as indicated by error bars, reflect the model variability in simulating aerosol transport.

856
857
858

859

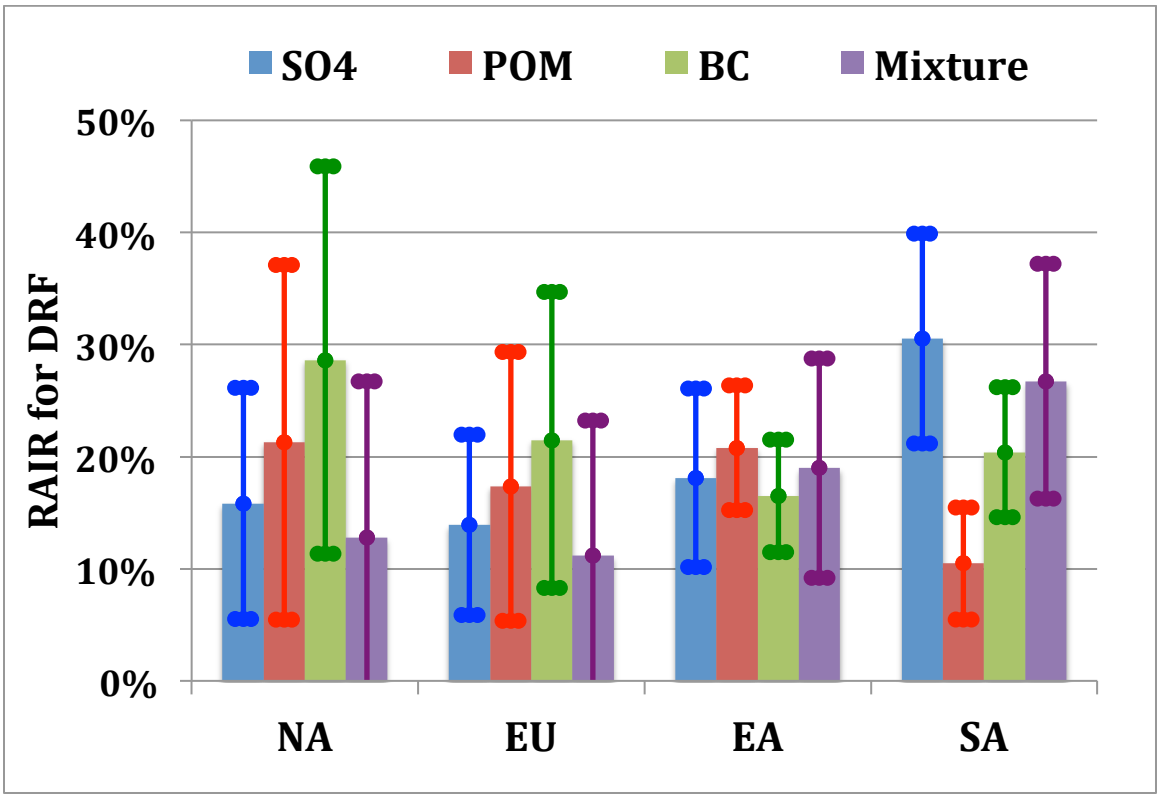

Figure 10: same as Figure 9 but for TOA all-sky DRF.

860